A Theoretical Study on the Gas Phase Reactions of the Anions NbO_3^-, NbO_5^-, and $NbO_2(OH)_2^-$ with H_2O and O_2

J. R. Sambrano,† L. Gracia, J. Andrés,* S. Berski,‡ and A. Beltrán

Departament de Ciències Experimentals, Universitat Jaume I, Box 224, 12080 Castelló, Spain, Department of Mathematics, Laboratorio de Simulação Molecular, Universidade Estadual Paulista, Box 473, 17033-360 Bauru, Brazil, and Faculty of Chemistry, University of Wroclaw, 14 F. Joliot-Curie Str., 50−383 Wroclaw, Poland

Received: June 25, 2004; In Final Form: September 27, 2004

The potential energy surfaces at the singlet (s) and the triplet (t) electronic states associated with the gas-phase ion/molecule reactions of **NbO_3^-**, **NbO_5^-**, and **$NbO_2(OH)_2^-$** with H_2O and O_2 have been investigated by means of DFT calculations at the B3LYP level. An analysis of the results points out that the most favorable reactive channel comprises **s-NbO_3^-** reacting with H_2O to give an ion−molecule complex **s-$NbO_3(H_2O)^-$** without a barrier. From this minima, an intramolecular hydrogen transfer takes place between the incoming water molecule and an oxygen atom of the **NbO_3^-** fragment to render the most stable minimum, **s-$NbO_2(OH)_2^-$**. This oxyhydroxide system reacts with O_2 along a barrierless process to obtain the triplet **t-$NbO_4(OH)_2^-$-A** intermediate, and the crossing point, CP1, between s and t electronic states has been characterized. The next step is the hydrogen-transfer process between the oxygen atom of a hydroxyl group and the one adjacent oxygen atom to render a minimum with the two OH groups near each other, **t-$NbO_4(OH)_2^-$-B**. From this point, the last hydrogen migration takes place, to obtain the product complex, **t-$NbO_5(H_2O)^-$**, that can be connected with the singlet separated products, **s-NbO_5^-** and H_2O. Therefore, a second crossing point, **CP2**, has been localized. The nature of the chemical bonding of the key minima (**NbO_3^-**, **$NbO_2(OH)_2^-$**, **$NbO_4(OH)_2^-$-B**, and **NbO_5^-**) in both electronic states of the reaction and an interaction with O_2 has been studied by topological analysis of Becke−Edgecombe electron-localization function (ELF) and atoms-in-molecules (AIM) methodology. The niobium−oxygen interactions are characterized as unshared-electron (ionic) interactions and some oxygen−oxygen interactions as protocovalent bonds.

1. Introduction

Transition metal oxides have gained increasing interest in the last years because of the prominent role played in the field of material science.[1] In particular, niobium oxide is one of the most important transition metal oxides and widely used in catalytic oxidation and surface corrosion processes.[2−21] During the course of these chemical reactions, different species such as niobium oxide clusters and the corresponding oxyhydroxide systems are formed. **NbO_3^-** undergoes an observable reaction with H_2O to form the dioxydihydroxide ion, **$NbO_2(OH)_2^-$**, while the reaction with O_2 to yield **NbO_5^-** occurs 2 or 3 orders of magnitude more slowly than the observable H_2O reactions. For this subject, it seems more feasible to obtain the pentoxide by adding O_2 to the **$NbO_2(OH)_2^-$** ion. This fact was analyzed in 1992 in a seminal study by Sigsworth and Castleman, Jr.,[2] where the gas-phase reactions of the anions **NbO_3^-**, **NbO_5^-**, and **$NbO_2(OH)_2^-$** with O_2, HCl, and H_2O were investigated in a fast-flow reactor. Moreover, reactions of **NbO_3^-** and $Nb_xO_y^-$ with methanol and ethanol were analyzed by Jackson et al.[11,12] using Fourier transform ion cyclotron resonance mass spectrometry combined with theoretical calculations based on the local spin-density approximation. On the basis of the observed reaction patterns, structures and reactivities of the ions have been proposed. However, despite the amount of experimental data regarding this subject, a detailed understanding of the molecular mechanism associated with the oxidation and hydration processes is still lacking.

Structural, energetic, and electronic characterization of intermediates and transition structures (TSs) cannot be achieved by using experimental procedures only. Accurate theoretical computations can offer an alternative source of information, and an interplay between theory and experiment is very helpful in this area of research. In addition, one can expect that different electronic states appear along the most favorable reactive channel; therefore, both singlet (s) and triplet (t) electronic states have been considered, and the corresponding crossing points (CPs) have been localized. In this sense, our ongoing interest in exploring how associated spin states affect the chemical reactivity of simple metal oxides is shown in a recent study on the reaction between VO_2^+ and C_2H_4 /C_2H_6.[22,23] Therefore, motivated by a desire to provide a bridge between experimental and theoretical works, we present a DFT study to elucidate the unclear molecular mechanism associated with the pathways started from $NbO_3^-/H_2O/O_2$ to all possible products, and we apply some innovative ideas on the bonding in such systems on the basis of the topological analysis of the electron localization function (ELF).[24] This theoretical approach opens new ways for a better understanding of the structure, energetics, and bonding properties of metal oxide clusters.[25−30]

The present paper addresses the nature of the molecular mechanism associated with the reaction of the anions **NbO_3^-**, **NbO_5^-**, and **$NbO_2(OH)_2^-$** with O_2 and H_2O involving s and t

* Author to whom correspondence may be sent. E-mail: Andres@uji.es.
† Universidade Estadual Paulista.
‡ University of Wroclaw.

10.1021/jp047229b CCC: $27.50
Published on Web 11/11/2004

electronic states. Attention is focused on the location of the CPs and the barrier heights associated with the interconversion of the oxides and oxyhydroxides, the relative stability, and the nature of chemical bonding, on the basis of ELF analysis, of the different minima on the potential energy surface (PES).

2. Theoretical Methods

All computations were carried out using the GAUSSIAN98 program package.[31] The calculations were performed at the unrestricted B3LYP level,[32,33] in combination with the standard all-electron 6-311++G(2d,p) [34] basis sets for O and H atoms and Hay−Wadt valence double-ζ (n+1) effective core potential set,[35] to represent Nb atoms. The reason that we adopted this level and basis set was that we applied it to calculate the complex molecular mechanisms associated with the reactions $VO_2^+ + C_2H_4$[22] and $VO_2^+ + C_2H_6$[23] and the tautomerization process of $MO(H_2O)^+$, M = V, Nb, and Ta[21] as well as previous works with complex systems involving vanadium oxide systems,[26,27,36] and they yielded satisfactory results. Therefore, we are confident with the data calculated at this computing level for this type of reaction.

The Berny algorithm has been employed for the geometry optimizations.[37] The computed stationary points have been characterized as minima or transition states by diagonalizing the Hessian matrix and analyzing the vibrational normal modes. The particular nature of the TSs has been determined by analyzing the motion described by the eigenvector associated with the imaginary frequency, the transition vector (TV).[38] Furthermore, the intrinsic reaction coordinate (IRC) method[39,40] has been used to describe minimum energy paths from TSs to the corresponding minima along the imaginary mode of vibration using the algorithm developed by González and Schlegel[41] in the mass-weighted internal-coordinate system. Thus, harmonic vibrational frequencies, zero-point and thermal-energy corrections, and force constants were calculated. The standard temperature (298.15 K) and pressure (1 atm) were used to obtain Gibbs free energies. The natural population analysis has been made by using the natural bond orbital (NBO).[42,43]

All coordinates were optimized in searches for the CPs between the two PESs in which DFT energies and gradients were calculated for each spin multiplicity. Starting from the stationary point closest to the crossing seams, the reaction pathway was traced down to the corresponding minimum. Thereafter, each optimized point along the reaction path was submitted to a single-point energy calculation with the other electronic state. In this way, we obtain the CP as the structures that have identical geometry and energy in the s and t hypersurfaces.

In addition, we have used the topological analysis of the chemical bond proposed by Silvi and Savin,[24] which relies upon the gradient field analysis of the ELF function, $\eta(\mathbf{r})$, of Becke and Edgecombe.[44] An exploration of its mathematical properties enables a partition of the molecular position space in basins of attractors, which present a one-to-one correspondence with chemical local objects such as bonds and lone pairs. These basins are either core basins, C(X), or valence basins, V(X,...), belonging to the outermost shell and characterized by their coordination number with core basins, which is called the synaptic order. From a quantitative point of view, the method allows the integration of the electron density over the basins to provide the basin populations, $\bar{N}$, and integrated spin densities $\langle S_z \rangle$. Moreover, increasing $\eta(\mathbf{r})$ enables the tree diagrams to be built reflecting the hierarchy of the basins. A description of the core region using the ELF method is missing in the calculation based on the pseudopotential approximation (PA). Because of this, additional calculations have been performed using all-electron basis sets [8s6p5d1f] proposed by Andrae et al.[45] for the Nb atom by means of single points calculations at geometrical structures optimized by the pseudopotential approximation. To check properties of the bond critical points (BCPs) localized on the gradient paths within the atoms-in-molecules (AIM) methodology, the ext94b module of the AIMPAC [46] suit of programs has been used. ELF calculations have been performed with the TopMod package,[47] and isosurfaces have been visualized with the program SciAn.[48]

3. Results and Discussion

3.1 Overview of the Stationary Points and Reaction Pathway. The selected geometrical parameters of the stationary points at s and t electronic states are depicted in Figure 1, while the Gibbs free energy profile (ΔG) is presented in Figure 2. Table 1 reports the results of the natural population analysis. Two combinations are possible for the reactants and products, depending on its particular electronic state. The most stable combination of reactants and products is formed by **s-NbO_3^-** ($^1A_1$) and **s-NbO_5^-** ($^1A'$), respectively, and H_2O, thus belonging to the overall singlet PES. The triplet-state combination, **t-NbO_3^-** ($^3A''$) and **t-NbO_5^-** ($^3A''$) + H_2O, stands 35.7 and 26.0 kcal/mol above the singlet.

An analysis of the potential energy surface for the **s/t-NbO_3^-** anion shows an interesting umbrella inversion motion for the **NbO_3^-** moiety. The corresponding TSs have a small value of the imaginary frequency, 415i and 285i cm^{-1} for s and t electronic states, respectively, while the barrier heights are around 12.5 and 18.7 kcal/mol, respectively. These facts strongly suggest that the ion is floppy at s and t states, and incoming molecules should not be significantly hindered by oxygen repulsions.[12]

In the first stage, a water molecule approaches the **s/t-NbO^{3-}** molecule, and the hydrated complex **s/t-$NbO_3(H_2O)^-$** is formed. In the s state, this movement implies a barrierless process and a gain of stability of 12.4 kcal/mol with respect to the separated reactants, while in the t state, it must overcome a barrier of 5.8 kcal/mol. A noticeable electronic charge transfer takes place from water to the trioxide anion, 0.12/0.10 au in s/t states, respectively. These values point out that the ion−molecule complex appears to be mostly electrostatic in nature.

The next step is associated with an intramolecular hydrogen transfer from the oxygen atom of the incoming water molecule to an oxygen atom of the trioxide fragment to yield the stable **s/t-$NbO_2(OH)_2^-$** intermediate (−59.0 and −17.8 kcal/mol in singlet and triplet states, respectively) via the transition structure **s/t-TS1**. This stationary point has an activation free energy computed with respect to the corresponding minimum of −1.0 and 2.4 kcal/mol, respectively. Both reaction pathways correspond to exothermic processes, with **s-$NbO_2(OH)_2^-$** being the most stable minimum.

The addition of **O_2** ($^3\Sigma_g$) to the **s/t-$NbO_2(OH)_2^-$** intermediate renders the **s/t-$NbO_4(OH)_2^-$-A** minimum. In the t state, this addition without barrier implies the formation of two additional Nb−O bonds (Nb−O_5 and Nb−O_6), and consequently, a noticeable electronic charge transfer to the Nb atom (0.54 au) is obtained. However, in the s state, the **O_2** molecule approaches the **s-$NbO_2(OH)_2^-$** intermediate without formation of any bond, overcoming a barrier of 39.8 kcal/mol. The intersystem crossing, via **CP1**, between the s and t PESs occurs in this stage of the

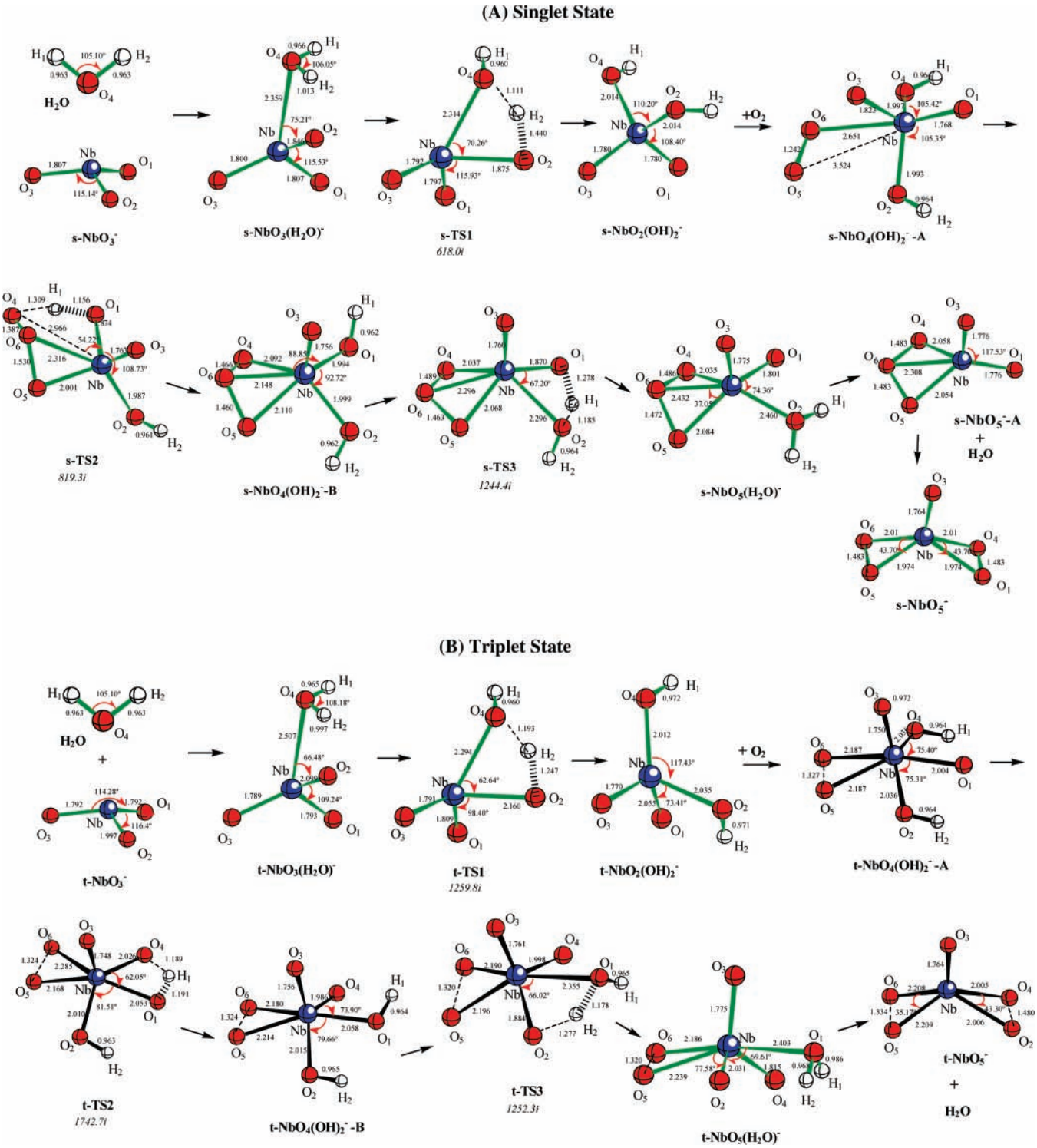

Figure 1. Structures (distances in Å and angles in degrees) of the stationary points at B3LYP/6-311++G(2d,p) level for H and O atoms and Hay−Wadt VDZ (n+1) ECP set to represent Nb atoms. For TSs, the imaginary vibrational frequencies (cm^{-1}) are shown in italics. (A) Singlet state and (B) triplet state.

reaction path connecting the **s-$NbO_2(OH)_2^-$** intermediate with the **t-$NbO_4(OH)_2^-$-A** minimum. The structure of the **CP1** is depicted in Figure 4. An analysis of the corresponding values shows that **CP1** is in a geometric and energetic middle position between **s-** and **t-$NbO_4(OH)_2^-$-A**. The O_5-O_6 distance in **s/t-$NbO_4(OH)_2^-$-A** is 1.242/1.327 Å and 1.295 Å in **CP1**. Also, the O_6-Nb/ O_5-Nb distances in **CP1** are 2.415/2.836 Å, respectively, compared to 2.651/3.524 Å in **s-$NbO_4(OH)_2^-$-A** and 2.187 Å in **t-$NbO_4(OH)_2^-$-A**. Accordingly, the energy of **CP1** is ca. 2.0 kcal/mol under/over **s/t-$NbO_4(OH)_2^-$-A**, respectively.

From **s/t-$NbO_4(OH)_2^-$-A**, different intramolecular hydrogen-transfer processes can take place between the oxygen atom of a hydroxyl group and the one adjacent oxygen atom, and then the two OH groups are near each other to render the **s/t-$NbO_4(OH)_2^-$-B** minima. In Figure 1, the corresponding TSs are depicted, **s/t-TS2**. The activation free energy of **s/t-TS2** computed with respect to the corresponding minima is 11.0 kcal/

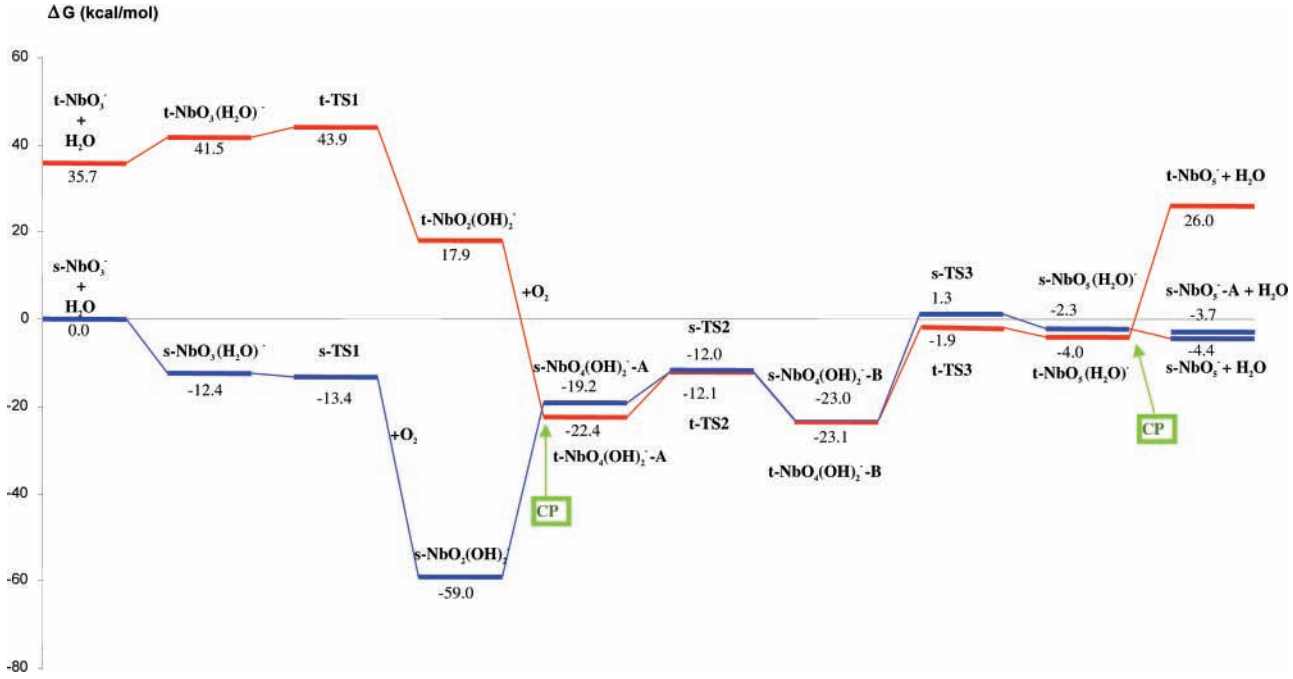

Figure 2. Gibbs free-energy profile, relative to the reactants in the singlet state. The total Gibbs free-energy value for the separated reactants is −509.090 799 hartrees.

TABLE 1: Natural Population Analysis for the Stationary Points: (A) Singlet State, (B) Triplet State

	Nb	O_1	O_2	O_3	O_4	H_1	H_2	O_5	O_6
				(A) Singlet State					
H_2O					−0.92	0.46	0.46		
s-NbO_3^-	2.05	−1.02	−1.02	−1.02					
s-$NbO_3(H_2O)^-$	2.05	−1.00	−1.10	−0.99	−0.96	0.48	0.52		
s-TS1	2.10	−0.98	−1.09	−0.97	−1.01	0.47	0.49		
s-$NbO_2(OH)_2^-$	2.11	−1.00	−1.07	−0.91	−1.08	0.46	0.49		
s-$NbO_4(OH)_2^-$-A	2.14	−0.89	−1.04	−0.82	−1.04	0.46	0.46	−0.17	−0.09
s-TS2	2.19	−1.00	−1.03	−0.89	−0.49	0.46	0.46	−0.57	−0.14
s-$NbO_4(OH)_2^-$-B	2.09	−0.96	−1.03	−0.85	−0.70	0.46	0.46	−0.26	−0.23
s-TS3	2.17	−1.05	−1.05	−0.86	−0.47	0.51	0.47	−0.57	−0.15
s-$NbO_5(H_2O)^-$	2.13	−1.00	−0.91	−0.91	−0.56	0.51	0.48	−0.61	−0.12
s-NbO_5^--A	2.13	−0.94		−0.93	−0.56			−0.56	−0.14
s-NbO_5^-	2.19	−0.56		−0.91	−0.56			−0.58	−0.58
				(B) Triplet State					
t-NbO_3^-	1.55	−0.95	−0.65	−0.95					
t-$NbO_3(H_2O)^-$	1.64	−0.95	−0.69	−0.96	−0.99	0.46	0.49		
t-TS1	1.65	−0.90	−0.65	−0.94	−1.07	0.46	0.45		
t-$NbO_2(OH)_2^-$	1.84	−0.70	−1.02	−0.93	−1.09	0.45	0.45		
t-$NbO_4(OH)_2^-$-A	2.10	−0.66	−1.00	−0.83	−1.00	0.46	0.46	−0.27	−0.27
t-TS2	2.13	−0.83	−1.02	−0.83	−0.82	0.46	0.46	−0.29	−0.25
t-$NbO_4(OH)_2^-$-B	2.09	−0.99	−1.04	−0.85	−0.64	0.46	0.46	−0.24	−0.26
t-TS3	2.06	−0.98	−1.04	−0.85	−0.63	0.46	0.48	−0.25	−0.26
t-$NbO_5(H_2O)^-$	2.01	−0.91	−0.66	−0.89	−1.00	0.52	0.49	−0.29	−0.27
t-NbO_5^-	1.76		−0.58	−0.93	−0.59			−0.33	−0.33

mol, higher than **s/t-TS1**. Between **s-** and **t-$NbO_4(OH)_2^-$-B** stationary points, geometrical differences are sensed. In the s state, an apparent trioxo bond is found, and a peroxo bond appears in the t state (see the ELF analysis in section 3.2). Therefore, it should be remarked that, at **s/t-$NbO_4(OH)_2^-$-A(B)** stationary points, it can be produced by an intramolecular scrambling process that implies consecutive hydrogen-transfer processes between neighbor oxygen atoms.

The final minimum **s/t-$NbO_5(H_2O)^-$** is achieved by the last hydrogen migration from O_1 to O_2 via **s-TS3**, or from O_2 to O_1 via **t-TS3**. In **s/t-TS3**, the distance of $Nb-O_2$ is increased from 1.999 to 2.296 Å, and the distance of $Nb-O_1$ is increased from 2.058 to 2.355 Å; the barrier heights associated with the third migration are substantial (24.3 and 21.2 kcal/mol, respectively), and the total charges of the water moieties are 0.06 and 0.08 au, respectively. Therefore, this intermediate can be viewed as a product complex and can be connected with the most stable separated products, **s-NbO_5^-** and H_2O. Therefore, at this point of the reaction path, there is another intersystem crossing between the s and t PESs, via **CP2**, that connects the **t-$NbO_5(H_2O)^-$** intermediate with the **s-NbO_5^-** product. The structure of the **CP2** is depicted also in Figure 4. An analysis of the corresponding values shows that **CP2** is in a geometric and energetic middle position between **s-** and **t-$NbO_5(H_2O)^-$**. The O_6-Nb-O_5 (singlet nomenclature) or O_5-Nb-O_2 (triplet nomenclature) bond angle is 50.0° in **CP2** when the bond angle is 37.5° in **s-$NbO_5(H_2O)^-$** and 77.6° in **t-$NbO_5(H_2O)^-$**. Also, the O_6-Nb/O_5-Nb (**s/t** nomenclature) distance in **CP2** is 2.315 Å compared to 2.432/2.239 Å in **s/t-$NbO_5(H_2O)^-$**. The symmetric **s-NbO_5^--A** minima is easily obtained from the **s-NbO_5-**

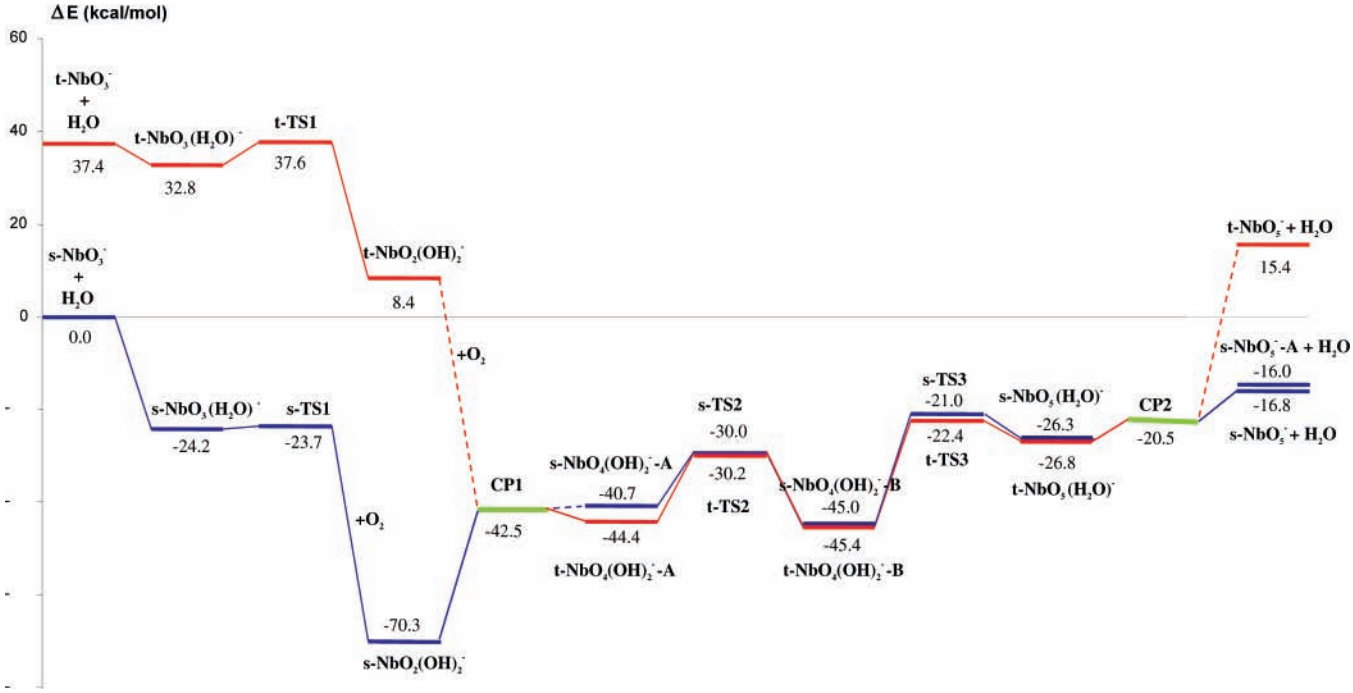

Figure 3. Relative energies ΔE (kcal/mol) with respect to the reactants in the singlet state. The total energy value for the separated reactants is −509.056 315 8 hartrees.

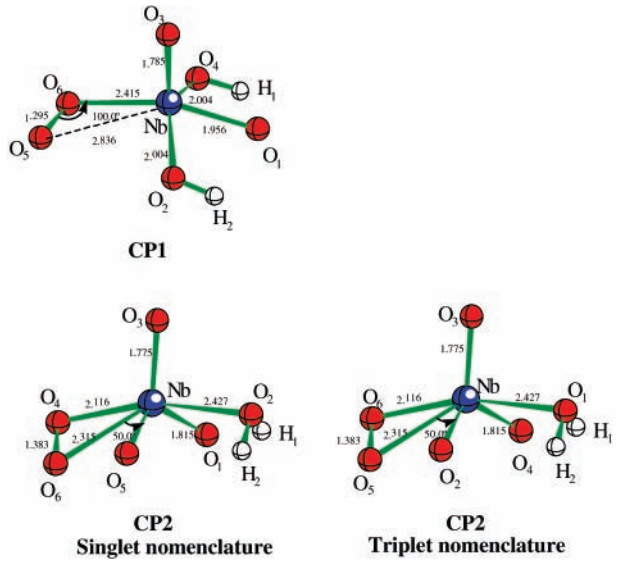

Figure 4. Structure of the crossing points found at B3LYP/6-311++G(2d,p) level for H and O atoms and Hay−Wadt VDZ (n+1) ECP set to represent Nb atoms.

TABLE 2: Relative Energies with Respect to Singlet Separated Reactants, ΔE (kcal/mol), and Thermodynamic Parameters, ΔG, ΔH, and $T\Delta S$ (kcal/mol): (A) Singlet State and (B) Triplet State

	ΔE	ΔG	ΔH	$T\Delta S$
(A) Singlet State				
s-$NbO_3(H_2O)^-$ + O_2	−24.24	−12.44	−22.92	−10.48
s-TS1 + O_2	−23.73	−13.39	−24.86	−11.46
s-$NbO_2(OH)_2^-$ + O_2	−70.25	−58.97	−69.54	−10.57
s-$NbO_4(OH)_2^-$-A	−40.71	−19.15	−39.20	−20.05
s-TS2	−30.02	−12.02	−35.33	−23.31
s-$NbO_4(OH)_2^-$-B	−45.04	−23.02	−45.06	−22.04
s-TS3	−20.98	1.32	−21.89	−23.21
s-$NbO_5(H_2O)^-$	−26.31	−2.28	−23.94	−21.66
s-NbO_5^--A + (H_2O)	−16.03	−3.70	−15.42	−11.75
s-NbO_5^- + (H_2O)	−16.82	4.40	−16.14	−11.74
(B) Triplet State				
t-NbO_3^- + (H_2O) + O_2	37.43	35.69	36.93	1.23
t-$NbO_3(H_2O)^-$ + O_2	32.77	41.55	33.33	−8.21
t-TS1 + O_2	37.59	43.95	34.63	−9.31
t-$NbO_2(OH)_2^-$ + O_2	8.43	17.92	8.49	−9.43
t-$NbO_4(OH)_2^-$-A	−44.35	−22.43	−43.06	−20.64
t-TS2	−30.16	−12.12	−33.84	−21.72
t-$NbO_4(OH)_2^-$-B	−45.44	−23.06	−44.04	−20.98
t-TS3	−22.38	−1.91	−23.57	−21.66
t-$NbO_5(H_2O)^-$	−26.78	−4.00	−24.76	−20.75
t-NbO_5^- + (H_2O)	15.42	26.00	−15.98	−10.02

$(H_2O)^-$ product complex. Both symmetric **s-NbO_5^--A** and **s-NbO_5^-** have similar energies. The nature of the chemical bonding of these reaction products is analyzed in section 3.2.

It is important to note that any attempt to locate transition structures for the **O_2** molecule addition to **s/t-NbO_3^-** or to **s/t-$NbO_2(OH)_2^-$** minima on a potential energy surface has been unsuccessful. In addition, the dihydroxide structures **s/t-$NbO_2(OH)_2^-$** and **s/t-$NbO_4(OH)_2^-$-A(B)** are more stable than the corresponding hydrated oxide ions **s/t-$NbO_3(H_2O)^-$** and **s/t-$NbO_5(H_2O)^-$**, respectively. This result is in agreement with previous works of Sambrano et al.[21] and Koyanagi et al. [49] on vanadium oxide cations, and Ricca and Bauschlicher [50] on $M(OH)_n^+$ systems for n = 1−3 and M = Sc, Ti, V, Co, Ni, and Cu. The global process can be dissected in terms of three consecutive proton transfers, along **s/t-TS1**, **s/t-TS2**, and **s/t-TS3**, with values of imaginary vibrational frequencies in the range 615i−1245i cm^{-1} (**s** state) and 1252i−1743i cm^{-1} (t state). Over the s PES, we can pay attention to the O_4 atom of the **s-TS2** structure, which reduces its negative charge from −1.04 to −0.49 au when H_1 is transferred, and at the same time, the charge of the O_5 atom is increased due to the formation of the O_5−Nb bond. However, in the t PES, the charge transferred along the hydrogen-transfer processes can be sensed in the corresponding minima after the transition states (see Table 1).

The obtained energetic values are schematically depicted in Figure 3. A comparison of Figures 2 and 3 (values of ΔE, ΔG, ΔH, and $T\Delta S$ summarized in Table 2) shows that the decrease in ΔG is smaller than the decrease of ΔE because of the entropic term, which disfavors the formation of cyclic structures. The

TABLE 3: ELF Values, $\eta(\mathbf{r})$, Basin Population $\bar{N}$, and Integrated Spin Densities $\langle S_z \rangle$ of the Key Minima Calculated at the DFT Level with the 8s6p5d1f Basis Set for Nb Atom (A) Singlet State and (B) Triplet State

(A) Singlet State

	s-NbO_3^-		s-$NbO_2(OH)_2^-$		s-$NbO_4(OH)_2^-$-B		s-NbO_5^--A		s-NbO_5^-	
	$\eta(\mathbf{r})$	$\bar{N}$	$\eta(\mathbf{r})$	$\bar{N}$	$\eta(\mathbf{r})$	$\bar{N}$	$\eta(\mathbf{r})$	$\bar{N}$	$\eta(\mathbf{r})$	$\bar{N}$
C(Nb)	1.000	38.25	1.000	38.13	1.000	38.15	1.000	38.26	1.000	38.28
$V_1(O_1)$	0.876	3.60	0.879	4.34	0.890	2.36	0.865	2.90	0.927	3.17
$V_2(O_1)$	0.876	3.55	0.863	2.77	0.891	3.74	0.881	4.17	0.925	3.22
$V_1(O_2)$	0.876	3.60	0.888	2.21	0.890	2.94				
$V_2(O_2)$	0.876	3.55	0.893	3.96	0.891	3.16				
$V_1(O_3)$	0.876	3.60	0.874	4.42	0.869[a]	6.99[a]	0.866	2.96	0.865[a]	7.02[a]
$V_2(O_3)$	0.876	3.55	0.861	2.63			0.879	4.06		
$V_1(O_4)$			0.888	2.21	0.921	3.13	0.922	3.13	0.927	3.17
$V_2(O_4)$			0.893	3.96	0.923	3.27	0.920	3.32	0.925	3.22
$V(H_1,O_4)$			1.000	1.45	1.000[b]	1.46[b]				
$V(H_2,O_2)$			1.000	1.45	1.000	1.45				
$V_1(O_5)$					0.923	3.26	0.922	3.15	0.915	3.05
$V_2(O_5)$					0.921	3.16	0.920	3.31	0.919	3.40
$V_1(O_6)$					0.934	2.72	0.944	3.21	0.915	3.05
$V_2(O_6)$					0.932	3.45	0.948	2.88	0.919	3.40
$V_{per}(O_1)/(O_4)$									0.654	0.20
$V_{per}(O_5)/(O_6)$									0.684	0.26
$V(O_4)/(O_6)$					0.616	0.07	0.631	0.07		
$V(O_5)/(O_6)$					0.624	0.07	0.631	0.07		

(B) Triplet State

	t-NbO_3^-			**t-$NbO_2(OH)_2^-$**			**t-$NbO_4(OH)_2^-$-B**			**t-NbO_5^-**		
	$\eta(\mathbf{r})$	$\bar{N}$	$\langle S_z \rangle$	$\eta(\mathbf{r})$	$\bar{N}$	$\langle S_z \rangle$	$\eta(\mathbf{r})$	$\bar{N}$	$\langle S_z \rangle$	$\eta(\mathbf{r})$	$\bar{N}$	$\langle S_z \rangle$
C(Nb)	1.000	38.83	0.50	1.000	38.47	0.62	1.000	38.15	0.01	1.000	38.82	0.46
$V_1(O_1)$	0.867	3.03	0.02	0.907	3.22	0.01						
$V_2(O_1)$	0.883	4.02	0.03	0.907	3.57	0.01						
$V_1(O_2)$	0.867	3.06	0.02	0.894	3.12	0.01	0.894	3.10	0.02	0.920	3.17	0.01
$V_2(O_2)$	0.883	4.01	0.03	0.888	2.91	0.01	0.891	2.99	0.01	0.920	3.09	0.01
$V_1(O_3)$	0.902	2.08	0.14	0.872[a]	7.08[a]	0.02[a]	0.872[a]	6.97[a]	0.01[a]	0.868[a]	7.06[a]	0.01[a]
$V_2(O_3)$	0.915	4.60	0.31									
$V_1(O_4)$				0.893[b]	6.18[b]	0.01[b]	0.907	3.15	0.19	0.920	3.17	0.01
$V_2(O_4)$							0.906	3.52	0.22	0.920	3.09	0.01
$V(H_1,O_4)$				1.000	1.46	0.01	1.000[c]	1.47[c]	0.01[c]			
$V(H_2,O_2)$				1.000	1.44	0.02	1.000	1.46	0.01			
$V_1(O_5)/(O_6)$							0.916	2.77	0.11	0.932	3.06	0.13
$V_2(O_5)/(O_6)$							0.927	3.15	0.14	0.919	2.80	0.11
$V_{per}(O_2)/(O_4)$										0.752	0.26	0.01
$V_{per}(O_5)/(O_6)$							0.751	0.28	0.01	0.822	0.40	0.01

[a] Attractor $V_1(O_3)$ corresponds to $V(O_3)$ in s-$NbO_2(OH)_2^-$, s-$NbO_4(OH)_2^-$, and s-NbO_5^- [b] Attractor $V(H_1,O_4)$ corresponds to $V(H_1,O_1)$ in s-$NbO_4(OH)_2^-$ [a] Attractor $V_1(O_3)$ corresponds to $V(O_3)$ in t-$NbO_2(OH)_2^-$, t-$NbO_4(OH)_2^-$, and t-NbO_5^- [b] Attractor $V_1(O_4)$ corresponds to $V(O_4)$ in t-$NbO_2(OH)_2^-$ [c] Attractor $V(H_1,O_4)$ corresponds to $V(H_1,O_1)$ in t-$NbO_4(OH)_2^-$

TABLE 4: Topological Data of Bond Critical Points (BCP) Localized for the Electron Density Gradient Field in the s-$NbO_4(OH)_2^-$-B Molecule; Only the Nb−O and O−O Bonds Were Investigated

BCP	$\rho(\mathbf{r})$ [au/bohr^3]	$\eta(\mathbf{r})$	$\nabla^2(\rho(\mathbf{r}))$ [au/bohr^5]	H [au/bohr^3]
Nb−O_1	0.123	0.324	0.358	−0.038
Nb−O_2	0.123	0.337	0.339	−0.038
Nb−O_3	0.225	0.456	0.498	−0.136
Nb−O_4	0.100	0.291	0.278	−0.026
Nb−O_5	0.096	0.281	0.271	−0.025
Nb−O_6	0.081	0.190	0.290	−0.016
O_4−O_6	0.237	0.605	0.360	−0.121
O_5−O_6	0.241	0.613	0.353	−0.125

TABLE 5: Topological Data of Bond Critical Points (BCP) Localized for the Electron Density Gradient Field in the s-NbO_5^--A Molecule

BCP	$\rho(\mathbf{r})$ [au/bohr^3]	$\eta(\mathbf{r})$	$\nabla^2(\rho(\mathbf{r}))$ [au/bohr^5]	H [au/bohr^3]
Nb−O_1	0.215	0.449	0.483	−0.125
Nb−O_3	0.214	0.442	0.496	−0.124
Nb−O_4	0.108	0.295	0.312	−0.031
Nb−O_5	0.108	0.295	0.312	−0.031
Nb−O_6				
O_4−O_6	0.226	0.602	0.348	−0.109
O_5−O_6	0.226	0.602	0.348	−0.109

enthalpic contribution, ΔH, is in the range of −69.5 to −15.4 kcal/mol in the s state (37.0 to −44.0 kcal/mol in the t state), while the entropic contribution, $T\Delta S$, goes from −23.3 to −10.5 kcal/mol (−21.7 to 1.2 kcal/mol in the t state).

3.2 Topological Analysis of ELF Function in the Key Minima. In Table 3 parts (A) and (B), topological data are collected for the key minima at s and t electronic states: the values of ELF at attractor, $\eta(\mathbf{r})$, the basin population, $\bar{N}$, and the integrated spin density, $\langle S_Z \rangle$. Attractor positions, ELF isosurfaces, and tree-bifurcation diagrams are presented for the **s-NbO_3^-**, **s-$NbO_2(OH)_2^-$**, **t-$NbO_4(OH)_2^-$-B**, **s-NbO_5^--A**, and **s-NbO_5^-** stationary points. Properties of the bond critical points (BCPs) for **s-$NbO_4(OH)_2^-$-B** and **s-NbO_5^--A** are collected in Tables 4 and 5.

***s/t-NbO_3^-*.** For the smallest system, **s/t-NbO_3^-**, similar topology of the ELF function was found in the s and t electronic states, owing to the number and type of attractors. The basin population of the Nb core equals 38.25 au (**s**) and 38.83 au (**t**), with atomic (topological) charges of +2.75 and +2.17 au, respectively. Only for the triplet state are there found two

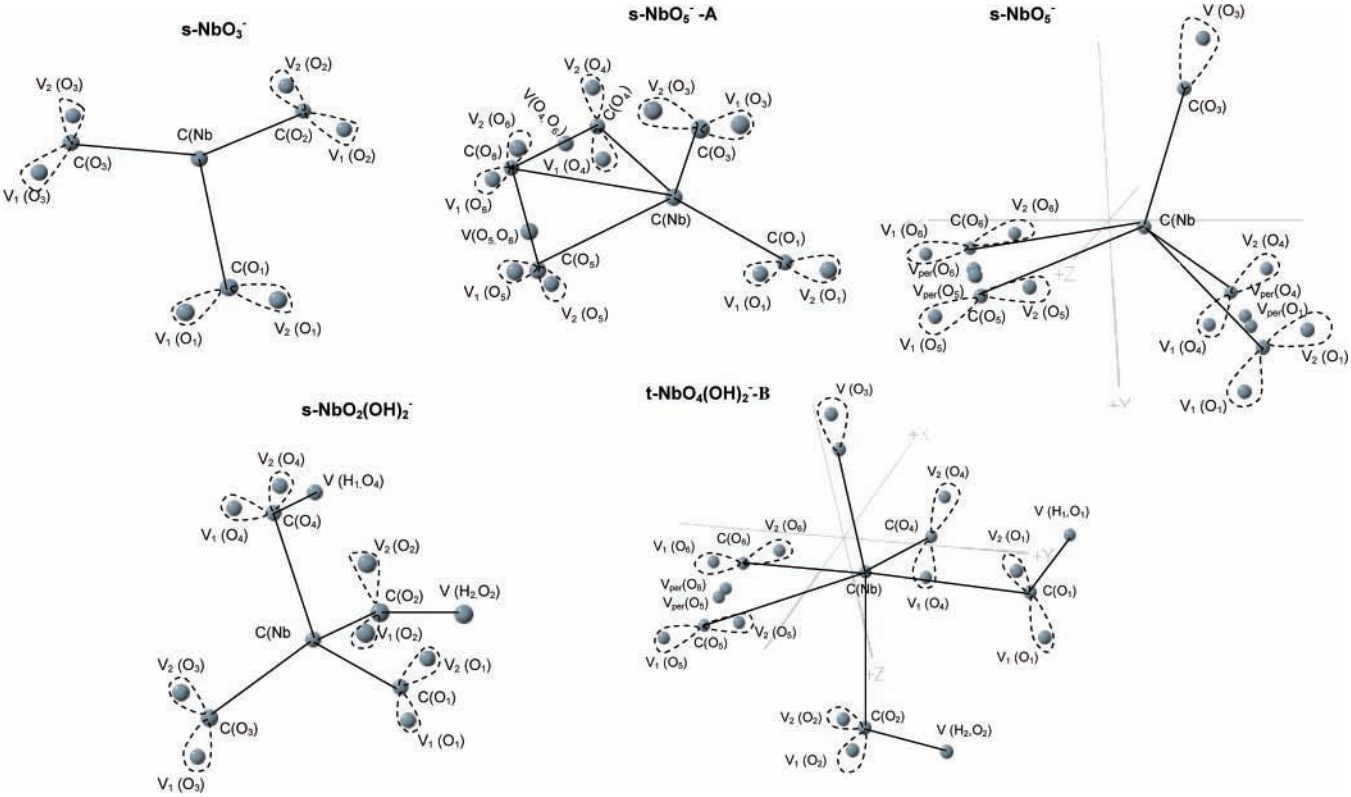

Figure 5. Attractor positions for **s-NbO$_3^-$**, **s-NbO$_2$(OH)$_2^-$**, **t-NbO$_4$(OH)$_2^-$-B**, **s-NbO$_5^-$-A**, and **s-NbO$_5^-$**, using the 8s6p5d1f basis set.

external core attractors, C_1(Nb) and C_2(Nb), which reflect a phenomenon of "core structuring" recently described by Kohout et al.[30] A main orbital contribution to $C_{i=1,2}$(Nb) basin of 0.21 au was determined to come from the molecular orbital number 34 mainly composed of the 4d atomic orbitals. In **t-NbO$_3^-$**, an unpaired electron density is concentrated mainly in the Nb core basin C(Nb) with one α-spin electron; the second unpaired electron is delocalized in nonbonding basins of oxygens. For oxygen atoms, there are localized core attractors C($O_{i=1,3}$) and a pair of monosynaptic valence attractors, V_1($O_{i=1,3}$) and V_2($O_{i=1,3}$), corresponding to the lone electron pairs. A binding between the Nb and $O_{i=1,3}$ atoms belongs to the unshared-electron type (ionic) because there are not any observed valence attractors V(Nb,$O_{i=1,3}$) of the disynaptic type. The respective attractors are presented in Figure 5 and the ELF isosurface in Figure 6. An analysis of ELF-topology in **s-NbO$_3^-$** by means of the tree-bifurcation diagrams reveals a first division of a reducible domain surrounding a whole molecule at $\eta(\mathbf{r}) = 0.40$ (Figure 7), divided into C(Nb) and three valence domains $V_{1\cup2}$($O_{i=1,3}$). The relatively large value of the separation of the C(Nb) core basin is typical for transition metal atoms. The latter splits at $\eta(\mathbf{r}) = 0.87$ into pairs of monosynaptic basins V_1($O_{i=1,3}$) and V_2($O_{i=1,3}$).

s/t-NbO$_2$(OH)$_2^-$. The topology of the ELF function in the **s/t-NbO$_2$(OH)$_2^-$** molecule is similar to that in **s/t-NbO$_3^-$**, with the exception of the H_1-O_4 bond present in the fourth coordination position and described by the C(O_4), V(O_4), V(H_1,O_4) basins and the H_2-O_2 bond with the protonated basin V(H_2,O_2). For the **s-NbO$_2$(OH)$_2^-$**, the respective attractors are also presented at Figure 5 and the ELF isosurface ($\eta = 0.78$) at Figure 6.

The Pauli repulsion between the nonbonding electron densities on the O_3 and O_4 atoms leads to a "formation" of only one monosynaptic basin V(O_3) in the triplet minimum **t-NbO$_2$-(OH)$_2^-$** instead of two V_1(O_3) and V_2(O_3) in the singlet. As before, only in the triplet state is the core polarization recognized

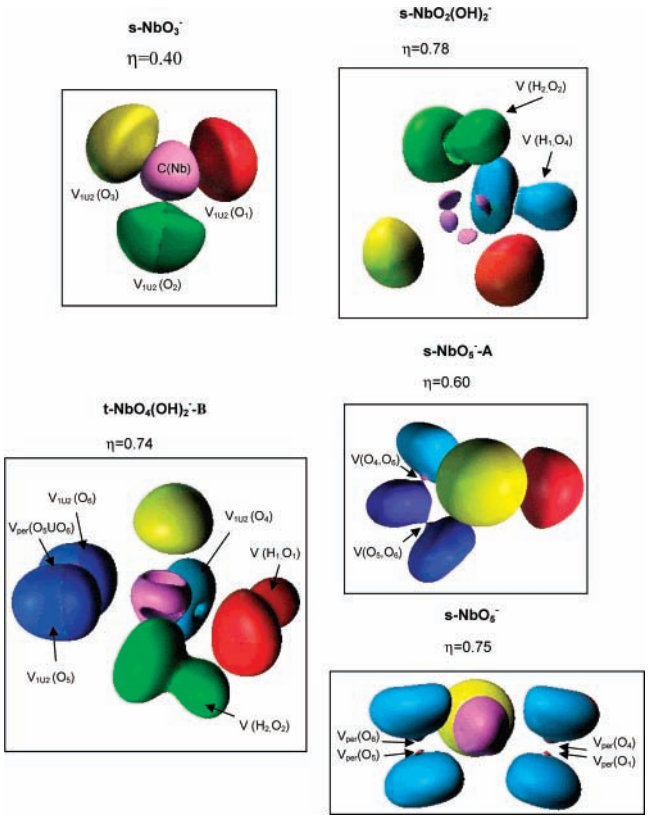

Figure 6. Electron localization function (ELF) isosurfaces for **s-NbO$_3^-$**, **s-NbO$_2$(OH)$_2^-$**, **t-NbO$_4$(OH)$_2^-$-B**, **s-NbO$_5^-$-A**, and **s-NbO$_5^-$**, using the 8s6p5d1f basis set.

with two $C_{i=1,2}$(Nb) external core attractors. The population of the core basins of Nb equals 38.47 au, which yields a topological charge of +2.6 au. The H−O bonds show the basin populations of 1.46 au for V(H_1,O_4) and 1.44 au for V(H_2,O_2). In cases of

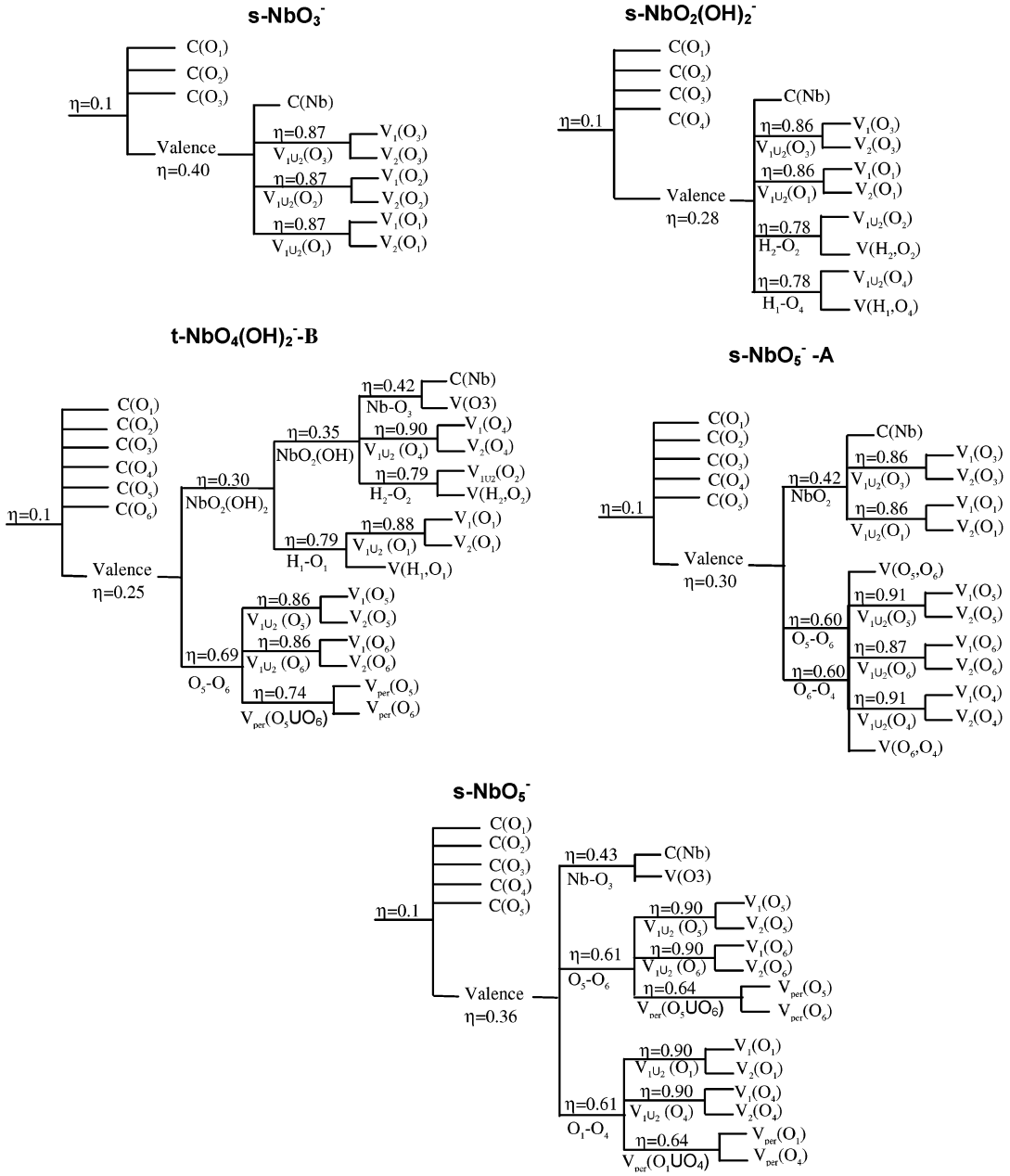

Figure 7. Localization domain reduction tree diagrams for **s-NbO_3^-**, **s-$NbO_2(OH)_2^-$**, **t-$NbO_4(OH)_2^-$-B**, **s-NbO_5^--A**, and **s-NbO_5^-**, using the 8s6p5d1f basis set.

the O_3 and O_4 atoms, only singular $V(O_3)$ and $V(O_4)$ basins are localized but with large populations of 7.08 and 6.18 au, respectively. The smaller $\bar{N}$ found for $V(O_4)$ is caused by a redistribution of the electron density of the H_1 atom (H_1-O_4 bond). For the symmetric **s-$NbO_2(OH)_2^-$**, the H−O bonds show the basin populations of 1.45 au, and the population of the basins $V_1(O_{i=1,4}) \cup V_2(O_{i=1,4})$ is similar, around 7.1 au.

s/t-$NbO_4(OH)_2^-$-B. In the triplet state, topological properties of the ELF function in **t-$NbO_4(OH)_2^-$-B** are similar to those in the **s/t-$NbO_2(OH)_2^-$** molecule, with the exception of the O_5-O_6 peroxo bond present in the five- and six-coordinate positions. A topological analysis of the ELF function for the prototype molecule O_2^{-2} containing the peroxo bond (Figure 8) shows that it is characterized by two monosynaptic basins $V_{per}(O_1)$ and $V_{per}(O_2)$ of the point type positioned between core basins $C(O_1)$ and $C(O_2)$. The nonbonding electron density is described by two circular monosynaptic valence attractors $V_1(O_{i=1,2})$ outside the molecule. From the point of view of the Catastrophe Theory, [51,52] such topology of ELF, primarily observed in studies

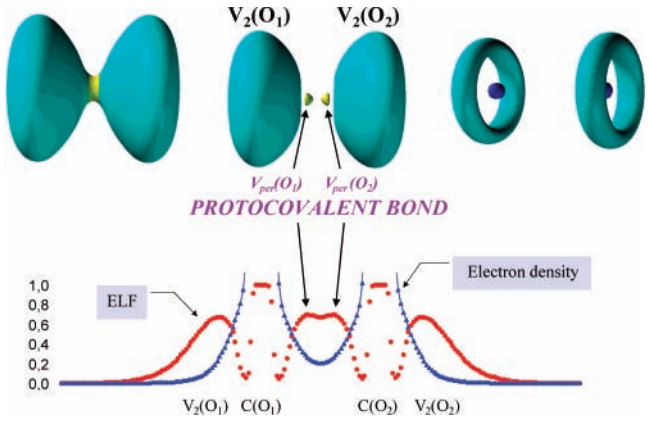

Figure 8. Topological analysis of the ELF function for prototype molecule O_2^{-2} containing the peroxo bond.

on the F_2 molecule by Llusar et al.,[53] corresponds to a forming/breaking of the covalent bond via the cusp catastrophe; therefore

the name "protocovalent bond" has been proposed. Until now, the protocovalent bond has been identified in all systems where y the peroxo bond is formally claimed.[26,54] The O_5-O_6 peroxo bond is described by the valence domains, $V_{1\cup2}(O_5)$, $V_{1\cup2}(O_6)$, and a small domain, $V_{per}(O_5) \cup V_{per}(O_6)$, which at $\eta(\mathbf{r}) \approx 0.74$ is separated into the $V_{per}(O_5)$ and $V_{per}(O_6)$ monosynaptic basins. The respective attractors are presented in Figure 3 and the ELF isosurface ($\eta(\mathbf{r})= 0.74$) in Figure 4. The population of the core basin of Nb equals 38.15e, which yields a topological charge of +2.85e. The H−O bonds show the basin populations of 1.47 au for $V(H_1,O_1)$ and 1.46 au for $V(H_2,O_2)$. In the case of the O_3 atom, only the singular $V(O_3)$ basin is localized with a large population of 6.97 au, whereas in the O_4 atom there are found two monosynaptic $V_{i=1,2}(O_4)$ caused by a redistribution of the electron density in the hydrogen-transfer process between the oxygen atom of a hydroxyl group (O_4) and the one adjacent oxygen atom (O_1), the latter with smaller $\bar{N}$ for $V_{i=1,2}(O_1)$, 3.10 and 2.99 au, respectively.

In **s-$NbO_4(OH)_2^-$-B**, the BCPs have been localized for all Nb−O_i bonds, therefore, Nb and O atoms are really bonded. According to positive values of the Laplacian of the electron density found for BCP and negative values of the total energy density, *H*, they may be characterized as covalent-depleted bonds. For the nonbonding electron density of oxygen, there are observed monosynaptic basins $V_i(O_j)$ with basin populations: $V_1(O_1) \cup V_2(O_1) = 6.1$ au, $V_1(O_2) \cup V_2(O_2) = 6.1$ au, $V_1(O_4) \cup V_2(O_4) = 6.4$ au, and singular basin $V(O_3)$ with 6.99 au. An atomic charge of Nb based on the topological analysis of ELF equals +2.85 au. The covalent type of interaction is found for the O−H bonds with $\bar{N}$ of 1.46 au being less populated than formal single bonds. An interesting mode of binding appears for three oxygen atoms $O_4-O_6-O_5$, which has been described as trioxo bonding. An analysis of the ELF function reveals two covalent disynaptic attractors $V(O_4,O_6)$ and $V(O_5,O_6)$ for $\eta(\mathbf{r}) = 0.617$ and 0.624, suggesting shared-electron interaction. However, the basin populations are very small (0.07e) with very large values of the relative fluctuations (0.97), and thus very large electron delocalization, which can be interpreted as very electron-poor O−O bonding.[55] In Table 4, there are collected topological data obtained for the bond critical points (BCP) for the gradient field of the electron density (the AIM method). Values of the Laplacian $\nabla^2\rho(\mathbf{r})$ of the electron density that are positive for the O_6-O_4 and O_6-O_5 bonds (0.360 and 0.353 [au/bohr^5]) show that the electron density around BCP is depleted, which is typical for the unshared-electron interactions. On the contrary, an examination of *H* for BCP reveals a dominance of the potential energy represented by negative values of *H* (−0.121 and −0.125 [au/bohr^3]), rather typical for the covalent interactions. In conclusion, the Nb−O bonds exhibit intermediate values between ionic and covalent bonds, which is typical for some Lewis acid−base interactions in a number of complexes, where the metal is a transition element with a zero or positive oxidation number and the ligand is neutral or ionic.

s/t-NbO_5^-. The last studied molecule is the product **s/t-NbO_5^-**, with a topology of the ELF function similar to those in the singlet and triplet electronic states in numbers and positions of localized valence attractors. For the triplet state, the core structuring in Nb is well visible, and the monosynaptic attractor C_1(Nb) can be localized. The bond exists between O_2-O_4 and O_5-O_6 pairs of atoms, and protocovalent bonds with $V_{per}(O_{i=2,4})$ and $V_{per}(O_{i=5,6})$ monosynaptic attractors support this statement. The nonbonding electron density of oxygen is described by monosynaptic attractors $V_{i=1,2}(O_{i=2,4})$ and $V_{i=1,2}(O_{i=5,6})$. For the valence electrons of the O_3 atom, only one monosynaptic $V(O_3)$ basin is found in comparison to two $V_{i=1,2}(O_3)$ basins in **s/t-NbO_3^-**. This is caused by the presence of the second pair of oxygen atoms, which in addition polarize the valence shell of O_3. The per-oxy bond O_1-O_4 exhibits 0.20 au (for the t state, the per-oxy bond O_2-O_4 is 0.26 au), and O_5-O_6 0.26 au (for the t state 0.40 au) with "protocovalent" $V_{per}(O_{i=2,4})$, $V_{per}(O_{i=5,6})$ attractors localized for smaller ELF values of 0.654, 0.684 (0.752,0.822 for the t state) than those found for other nonbonding attractors. The population of core basins, that is, C(Nb) and C_1(Nb) of 38.82e, yields a positive topological charge of 2.18 au for the **t-NbO_5^-** and 2.72 au for the **s-NbO_5^-**.

s-NbO_5^--A. Localized core and valence attractors are exhibited in Figure 5 and ELF surface in Figure 6. The Nb−O bonds are dominated by the electrostatic interactions since V(Nb,O) attractors are observed. The topological atomic charge of Nb equals +2.74 au. The electron density transferred from the Nb atom is mainly concentrated in the valence shell of oxygen atoms with the basin populations as follows: $V_1(O_1) \cup V_2(O_1) = 7.07$ au, $V_1(O_2) \cup V_2(O_2) = 6.45$ au, $V_1(O_4) \cup V_2(O_4) = 6.46$ au, and singular basin $V_1(O_3)$ of 6.99 au. A bonding in the trioxo $O_4-O_6-O_5$ fragment is reflected by two covalent disynaptic attractors $V(O_4,O_6)$ and $V(O_5,O_6)$ localized at $\eta(\mathbf{r}) = 0.631$ and $\rho(\mathbf{r}) = 0.286$ [au/bohr^3]. Similar to the **s-$NbO_4(OH)_2^-$-B** minimum, the population of the $V(O_4,O_6)$ and $V(O_5,O_6)$ basins is very small (0.07e) with very large values of relative fluctuation, 0.97, indicating very large delocalization of the electron density. The topological analysis of the electron density (Table 5) reveals the BCPs localized on the gradient paths linking oxygen nuclei for $\rho(\mathbf{r}) = 0.226$ [au/bohr^3], confirming that they are indeed bound. A positive value of the Laplacian $\nabla^2(\rho(\mathbf{r}) = 0.348$ [au/bohr^5] and the total energy density $H = -0.109$ [au/bohr^3] imply that the bonding is between the covalent and ionic type or *covalent depleted*.[55] BCPs with similar properties are found for the Nb−O bonds. An exception is the Nb−O_4 interaction for which BCP has not been observed, and it corresponds to the largest separation between the Nb and O atoms of 2.308Å.

4. Conclusions

The chemical rearrangements between **NbO_3^-**, **NbO_5^-**, and **$NbO_2(OH)_2^-$** and **O_2** and **H_2O** have been computed and analyzed. The potential energy surfaces in the singlet and triplet electronic states have been characterized in detail at the B3LYP level with all electron 6-311++G(2d,p) basis sets for O and H atoms and Hay−Wadt valence double-ζ (n+1) effective core potential set to represent Nb atoms. The reaction pathway is obtained, characterizing the crossing points between both surfaces, and the behavior along the path has been supported by a topological description on the basis of the gradient field analysis of the ELF function of all the key minima to characterize the chemical bonding. The main results are summarized as follows:

(i) The reaction pathway is associated with an exothermic process along an inverted energy profile via two intersystem crossing points **CP1** and **CP2** between s and t PESs.

(ii) The reaction pathways can be dissected as three consecutive hydrogen-transfer processes, and three associated transition structures (**s/t-TS1**, **s/t-TS2**, and **s/t-TS3**) have been characterized on PES with values of imaginary vibrational frequencies in the range of 615i−1245i cm^{-1} in the s state and of 1252i−1743i cm^{-1} in the t state.

(iii) The dihydroxide structures **s/t-$NbO_2(OH)_2^-$** and **s/t-$NbO_4(OH)_2^-$-A(B)** are the most stable minima on PES, and in

agreement with previous works, they are more stable than the corresponding hydrated oxide ions **s/t-$NbO_3(H_2O)^-$** and **s/t-$NbO_5(H_2O)^-$**. Moreover, at **s/t-$NbO_4(OH)_2^-$-A(B)** stationary points, an intramolecular scrambling process take place that implies hydrogen-transfer processes between neighboring oxygen atoms.

(iv) The ELF topology in the smallest system **NbO_3^-** in the s and t electronic states is similar with more marked core structuring in the triplet state. For oxygen atoms, there are localized core attractors $C(O_{i=1,3})$ and pairs of monosynaptic valence $V_1(O_{i=1,3})$ and $V_2(O_{i=1,3})$ attractors corresponding to the lone electron pairs. In **s/t-$NbO_2(OH)_2^-$**, protonated basins $V(H_2,O_2)$ and (H_1-O_4) appear, characterizing covalent bonds H_2-O_2 and H_1-O_4. In the **t-$NbO_4(OH)_2^-$-B** minimum, the O_5-O_6 peroxo bond is observed with nonbonding basins $V_{1\cup2}(O_5)$, $V_{1\cup2}(O_6)$, and small domain $V_{per}(O_5) \cup V_{per}(O_6)$, which at $\eta \approx 0.74$ is separated into the $V_{per}(O_5)$ and $V_{per}(O_6)$ monosynaptic basins; in **s-$NbO_4(OH)_2^-$-B**, three oxygen atoms $O_4-O_6-O_5$ form the trioxo bonding. In **s/t-NbO_5^-**, there are two per-oxy bonds O_2-O_4 and O_5-O_6 described by pairs of monosynaptic attractors $V_{per}(O_{i=2,4})$, $V_{per}(O_{i=5,6})$.

(v) On the basis of the topological analysis of the electron localization function (ELF), all Nb−O bonds belong to the unshared electron type dominated by the electrostatic interactions and to the *covalent-depleted* type using topological analysis of the electron density (the AIM methodology). The trioxo bonding $O_i-O_j-O_k$ possesses properties of the covalent bonds with bonding disynaptic attractors $V(O_i,O_j)$, $V(O_j,O_k)$ but with very small basin populations (0.07e) and very large delocalization (the relative fluctuation of 0.97), which correspond well to the *covalent-depleted* characteristic obtained from the AIM method. The peroxo bonds are recognized as the protocovalent bonds.

(vi) For **NbO_3^-**, **$NbO_2(OH)_2^-$**, and **NbO_5^-** molecules in the triplet state, there are found external core attractors $C_{i=1,2}(Nb)$ that reflect a phenomenon of "core structuring"; the population of core basins yields positive topological charges of 2.75/2.17, 2.87/2.53, 2.85/2.85, and 2.72/2.18 au for **s/t-NbO_3^-**, **s/t-$NbO_2(OH)_2^-$**, **s/t-$NbO_4(OH)_2^-$-B**, and **s/t-NbO_5^-**, so that the eight species are polar ions with a charge-depleted metal center, according to theoretical studies of A. Dinca et al.[56]

Acknowledgment. This work is supported by DGI, (L.G. thanks the Ministerio de Ciencia y Tecnología (BQU2000-1425-C03-02) as well as the Fundació Bancaixa (P1A2002-05). J.R.S. thanks the Brazilian Funding Agencies FAPESP, CAPES, and Fundació Bancaixa. S.B. is grateful to the Wroclaw Centre for Networking and Supercomputing for the granted time, and to The Marie Curie Development Host Fellowship program (HPMD-CT-2000-00055). The constructive comments of the reviewers are gratefully acknowledged.

References and Notes

(1) Henrich, V. E.; A., C. P. In *The Surface Science of Metal Oxides*; Kung, H. H., Ed.; Elsevier: Amsterdam, The Nederlands, 1989; Cambridge University Press: New York, 1994; Vol. 45.

(2) Sigsworth, S. W.; Castleman, A. W. *J. Am. Chem. Soc.* **1992**, *114*, 10471−10477.

(3) Pittman, R. M.; Bell, A. T. *J. Phys. Chem.* **1993**, *97*, 12178−12185.

(4) Obara, K.; Iwasaki, K.; Matushima, S.; Hirose, T.; Shioga, M.; Suemoto, Y. *Catal. Today* **1996**, *28*, 183−189.

(5) Deng, H. T.; Kerns, K. P.; Castleman, A. W. *J. Phys. Chem.* **1996**, *100*, 13386-13392.

(6) Deng, H. T.; Kerns, K. P.; Bell, R. C.; Castleman, A. W. *Int. J. Mass Spectrom.* **1997**, *167*, 615−625.

(7) Mwakapumba, J.; Ervin, K. N. *Int. J. Mass Spectrom. Ion Processes* **1997**, *161*, 161−174.

(8) Zhou, M. F.; Andrews, L. *J. Phys. Chem. A* **1998**, *102*, 8251−8260.

(9) Anokhina, E. V.; Essig, M. W.; Day, C. S.; Lachgar, A. *J. Am. Chem. Soc.* **1999**, *121*, 6827−6833.

(10) Wu, Q. F.; Yang, S. H. *Int. J. Mass Spectrom.* **1999**, *184*, 57−65.

(11) Jackson, P.; Fisher, K. J.; Willett, G. D. *Chem. Phys.* **2000**, *262*, 179−187.

(12) Jackson, P.; Fisher, K. J.; Willett, G. D. *Int. J. Mass Spectrom.* **2000**, *197*, 95−103.

(13) Westmacott, G.; Zhong, F.; Frank, M.; Friedrich, S.; Labov, S. E.; Benner, W. H. *Rapid Commun. Mass Spectrom.* **2000**, *14*, 600−607.

(14) Majumdar, D.; Balasubramanian, K. *J. Chem. Phys.* **2001**, *115*, 885−898.

(15) Green, S. M. E.; Alex, S.; Fleischer, N. L.; Millam, E. L.; Marcy, T. P.; Leopold, D. G. *J. Chem. Phys.* **200**1, *114*, 2653−2668.

(16) Vakhtin, A. B.; Sugawara, K. *J. Chem. Phys.* **2001**, *115*, 3629−3639.

(17) Zemski, K. A.; Justes, D. R.; Castleman, A. W. *J. Phys. Chem. A* **2001**, *105*, 10237−10245.

(18) Zemski, K. A.; Justes, D. R.; Bell, R. C.; Castleman, A. W. *J. Phys. Chem. A* **2001**, *105*, 4410−4417.

(19) Santos, I.; Loureiro, L. H.; Silva, M. F. P.; Cavaleiro, A. M. V. *Polyhedron* **2002**, *21*, 2009−2015.

(20) Nowak, L.; Page, E. M.; Rice, D. A.; Richardson, A. D.; French, R. J.; Hedberg, K.; Ogden, J. S. *Inorg. Chem.* **2003**, *42*, 1296−1305.

(21) Sambrano, J. R.; Andrés, J.; Gracia, L.; Safont, V. S.; Beltrán., A. *Chem. Phys. Lett.* **2004**, *384*, 56−62.

(22) Gracia, L.; Sambrano, J. R.; Safont, V. S.; Calatayud, M.; Beltrán, A.; Andrés, J. *J. Phys. Chem. A* **2003**, *107*, 3107−3120.

(23) Gracia, L.; Andrés, J.; Sambrano, J. R.; Safont, V. S.; Beltrán, A. *Organometallics* **2004**, *23*, 730−739.

(24) Silvi, B.; Savin, A. *Nature* **1994**, *371*, 683.

(25) Sambrano, J. R.; Andrés, J.; Beltrán, A.; Sensato, F.; Longo, E. *Chem. Phys. Lett.* **1998**, *287*, 620−626.

(26) Calatayud, M.; Andrés, J.; Beltrán, A.; Silvi, B. *Theor. Chem. Acc.* **2001**, *105*, 299−308.

(27) Calatayud, M.; Silvi, B.; Andrés, J.; Beltrán, A. *Chem. Phys. Lett.* **2001**, *333*, 493−503.

(28) Chiodo, S.; Kondakova, O.; Michelini, M. D.; Russo, N.; Sicilia, E. *Inorg. Chem.* **2003**, *42*, 8773−8782.

(29) Chiodo, S.; Kondakova, O.; Michelini, M. D.; Russo, N.; Sicilia, E.; Irigoras, A.; Ugalde, J. M. *J. Phys. Chem. A* **2004**, *108*, 1069−1081.

(30) Kohout, M.; Wagner, F. R.; Grin, Y. *Theor. Chem. Acc.* **2002**, *108*, 150−156.

(31) Frisch, M. J.; Trucks, G. W.; Schlegel, H. B.; Scuseria, G. E.; Robb, M. A.; Cheeseman, J. R.; Zakrzewski, V. G.; Montgomery, J. A.; Stratmann, R. E.; Burant, J. C.; Dapprich, S.; Millam, J. M.; Daniels, A. D.; Kudin, K. N.; Strain, M. C.; Farkas, O.; Tomasi, J.; Barone, V.; Cossi, M.; Cammi, R.; Mennucci, B.; Pomelli, C.; Adamo, C.; Clifford, S.; Ochterski, J.; Petersson, G. A.; Ayala, P. Y.; Cui, Q.; Morokuma, K.; Malick, D. K.; Rabuck, A. D.; Raghavachari, K.; Foresman, J. B.; Cioslowski, J.; Ortiz, J. V.; Stefanov, B. B.; Liu, G.; Liashenko, A.; Piskorz, P.; Komaromi, I.; Gomperts, R.; Martin, R. L.; Fox, D. J.; Keith, T.; Al-Laham, M. A.; Peng, C. Y.; Nanayakkara, A.; Gonzalez, C.; Challacombe, M.; Gill, P. M. W.; Johnson, B. G.; Chen, W.; Wong, M. W.; Andres, J. L.; Head-Gordon, M.; Replogle, E. S.; Pople, J. A. *Gaussian 98*, revision A.1; Gaussian, Inc.: Pittsburgh, PA, 1998.

(32) Lee, C.; Yang, R. G.; Parr, R. G. *Phys. Rev. B* **1988**, *37*, 785−789.

(33) Becke, A. D. *J. Chem. Phys.* **1993**, *98*, 5648.

(34) Pople, J. A.; Head-Gordon, M.; Raghavachari, K. *J. Chem. Phys.* **1987**, *87*, 5968.

(35) Hay, P. J.; Wadt, W. R. *J. Chem. Phys.* **1985**, *82*, 299.

(36) Calatayud, M.; Andrés, J.; Beltrán, A. *J. Phys. Chem. A* **2001**, *105*, 9760−9775.

(37) Schlegel, H. B. *J. Comput. Chem.* **1982**, *3*, 214−218.

(38) McIver, J. W., Jr. *Acc. Chem. Res.* **1974**, *7*, 72.

(39) Fukui, K. *J. Phys. Chem.* **1970**, *74*, 4161.

(40) González, C.; Schlegel, H. B. *J. Chem. Phys.* **1989**, *90*, 2154.

(41) González, C.; Schlegel, H. B. *J. Phys. Chem.* **1990**, *94*, 5523.

(42) Reed, A. E.; Weinstock, R. B.; Weinhold, F. *J. Chem. Phys.* **1985**, *83*, 735.

(43) Reed, A. E.; Curtiss, L. A.; Weinhold, F. *Chem. Rev.* **1988**, *88*, 899.

(44) Becke, A. D. E., K. E. *J. Chem. Phys.* **1990**, *92*, 5397.

(45) Andrae, D.; Haeussermann, U.; Dolg, M.; Stoll, H.; Preuss, H. *Theor. Chim. Acta* **1990**, *77*, 123.

(46) Bader, R. F. W. *Atoms in Molecules: A Quantum Theory*; Oxford University Press: Oxford UK, 1990.

(47) Noury, S. K., Krokidis, X.; Fuster, F.; Silvi, B. *TopMod Package*; Universite Pierre et Marie Curie: Paris, 1997.

(48) Pepke, E.; Muray, J.; Lyons, J. *Scian* (Supercomputer Computations Research Institute); Florida State University: Tallahassee, FL, 1993.

(49) Koyanagi, G. K.; Caraiman, D.; Blagojevic, V.; Bohme, D. K. *J. Phys. Chem. A* **2002**, *106*, 4581−4590.

(50) Ricca, A.; Bauschlicher, C. W. *J. Phys Chem. A* **1997**, *101*, 8949−8955.

(51) Thom, R. *Stabilité Structurelle et Morphogénèse*; *W. A. Benjamin, Inc.*: Paris, 1972.

(52) Poston, T.; Stewart, I. *Catastrophe Theory and Its Applications*; Dover Publications: New York, 1996.

(53) Llusar, R.; Beltrán, A.; Andrés, J.; Noury, S.; Silvi, B. *J. Comput. Chem.* **1999**, *20*, 1517.

(54) Calatayud, M.; Berski, S.; Beltrán, A.; Andrés, J. *Theor. Chem. Acc.* **2002**, *108*, 12−20.

(55) Bill, A.; Latajka, Z. *Chem. Phys.* **2004**, *303*, 43−53.

(56) Dinca, A.; Davis, T. P.; Fisher, K. J.; Smith, D. R.; Willett, G. D. *Int. J. Mass Spectrom.* **1998**, *182/183*, 73−84.